ORIGINAL ARTICLE

Effect of dynamic spreading and the disperse phase of crystalline starch nanoparticles in enhancing oil recovery at reservoir condition of a typical sarawak oil field

Augustine Agi[1] · Radzuan Junin[1,2] · Azza Abbas[1,3] · Afeez Gbadamosi[1] · Nur Bashirah Azli[1]

Abstract

Nanofluid flooding has been proven to be very effective in enhanced oil recovery (EOR). The performance depends on the material and formulation process. Previous studies have focused only on the use of inorganic, metal and metal oxides nanoparticles. The use of nanofluids from natural sources has not been investigated to a reasonable extent for possible application in EOR. In this study, ascorbic acid was used for the first time to synthesize crystalline starch nanoparticles (CSNP). The physical properties of the CSNP including their size distribution and crystalline structures were investigated. The interfacial properties of the crystalline starch nanofluid (CSNF) at the interface of oil and water (O/W) were investigated at different concentrations and temperatures. The effect of the interaction between electrolyte and ultrasonic was determined. The wettability alteration efficiency of CSNF on oil-wet sandstone surface was investigated using the sessile drop method. A core flooding experiment was conducted at reservoir conditions to justify the effect of wettability alteration and dispersion of CSNF on additional oil recovery. The performance of the CSNF was compared with the conventional EOR chemical. The methods were effective in producing spherical and polygonal nanoparticles with a mean diameter of 100 nm and increased in crystallinity of 7%. The interfacial tension (IFT) decreased with increase in concentration of CSNF, electrolyte and temperature. The results show that CSNF can change the wettability of sandstone at low concentration, high salinity and elevated temperature. The pressure drops data show stability of CSNF at 120 °C. The formation of oil bank was enough to increase oil recovery by 23%. CSNF was effective in mobilizing residual oil at reservoir condition. It can, therefore, be concluded from this experiment work that the method applied herein is easier, cost-effective and can reduce energy consumption making the method economically advantageous compared to conventional methods.

Keywords Ultrasonic · Nanoparticles · Cassava starch · Synthesis · Wettability · IFT · Enhanced oil recovery

Introduction

Although there is clamour for renewable energy, the dawn of this century has seen an increasing demand for fossil fuel. But the production from most oil fields around the world is declining because of high capillary forces and heterogeneity of the reservoir leading to early abandonment (Kumar and Mandal 2018; Agi et al. 2018a). Wettability can affect oil saturation and total oil recovery. It controls the oil flow and distribution of fluid (Giraldo et al. 2013). About 50% of the reservoirs around the world are typically oil/intermediate-wet (Al-Anssari et al. 2017). The challenge is to recover this trapped oil economically and delay the abandonment. Water flooding of oil-wet rocks is not effective as water cannot imbibe into the rock matrix resulting in low productivity (10–30%). The change in wettability of rocks can allow

✉ Radzuan Junin
  r-razuan@utm.my

1 Department of Petroleum Engineering, Faculty of Engineering, School of Chemical and Energy Engineering, Universiti Teknologi Malaysia, 81310 Johor Bahru, Malaysia

2 Institute for Oil and Gas, Universiti Teknologi Malaysia, 81310 Johor Bahru, Malaysia

3 School of Computing, Engineering and Technology, Asia Pacific University of Technology and Innovation (APU), 57000 Kuala Lumpur, Malaysia

water to imbibe into the matrix of the rock and displace oil from the pores.

Nanotechnology is one of the most innovative technologies of this decade; nanoparticles are used to develop a kind of novel environment-friendly slurries, which are used to fabricate high-performance substrate in semiconductor industries (Zhang et al. 2016, 2017a, b, 2018, 2019). They are also used to develop new diamond wheels and machining approaches to fabricate high-performance devices (Zhang et al. 2015a, b; Wang et al. 2018). With the use of nanoparticles in the industries, nanoscale precision surfaces are fabricated, which is extremely significant for high-performance materials widely used in electronic industries (Zhang et al. 2012a, b, c, 2013a, b, 2017b; Wang et al. 2018). Therefore, the tailoring of chemicals and formulation of chemical slugs is seen as a lasting solution to the numerous problems plaguing the oil and gas industry (Kumar and Mandal 2018; Agi et al. 2018b). This is because nanoparticles can localize at oil–water (O/W) interface and reduce residual oil saturation. Experimental results have shown that nanoparticles can reduce the interfacial tension (IFT) by 33–42% compared to brine (Bayat et al. 2014; Kumar and Mandal 2018). Several authors (Giraldo et al. 2013; Al-Anssari et al. 2017) have reported that nanofluid can significantly change the rock surface wettability. Giraldo et al. (2013) reported that nanofluid can alter the wettability of sandstone cores. The efficiency of nanofluid in altering wettability is due to the solid surface chemistry in relationship to the nanoparticles type. The surface modification of the solid surface is dependent on the nanofluid composition. However, with the excellent results reported by previous studies, environmental and economic factors have impeded the full-scale field application (Agi et al. 2018b). With increased demand for energy and inaccessibility to oil deposits, it is important that effective, economically and environmentally friendly alternatives, such as nanoparticles derived from natural source are considered (Agi et al. 2018a).

Starch is a renewable natural polymer abundant in nature; its granules are made up of rigid structural layers of crystalline and amorphous lamella (Ye et al. 2017). Crystalline starch nanoparticles (CSNP) can be obtained by hydrolysis of the amorphous areas (Ye et al. 2017). This approach can produce nanoparticles 5–7 nm in size, but the drawback is the long duration and low yield of the nanoparticles (Shahrodin et al. 2015). Also, the use of chemical is a source of concern as nanoparticles obtained from strong acid can aggregate making them less suitable for industrial applications (Dufresne 2008). Physical treatment such as ultrasonic is a very effective method for the physical disruption of cellular structures (Suslick 2001). The exposure of the natural polymers solution to high-intensity ultrasonic can reduce the molar mass. The preparation time becomes shortened and the ultrasound can effectively prevent aggregation. However,

Kim et al. (2013) reported disruption of the nanoparticle's crystallinity by ultrasonic. But, the modification and intensification of the process parameters and homogenization can also enhance crystallinity by ultrasonic (Kim et al. 2013). If the crystallinity of nanoparticles is preserved after treatment, the powder products could be readily obtained and their accessibility to industrial items such as composites, nano-fillers, emulsifiers, viscocifiers and stabilizers could be improved.

Nanofluid flooding has been proven to be very effective in enhanced oil recovery (EOR). The performance depends on the material and formulation process. Previous studies have focused on the use of inorganic, metal and metal oxide nanoparticles. However, the use of nanofluid from natural source for EOR has not been investigated to a reasonable extent. Therefore, in this study ascorbic acid was used for the first time to synthesize CSNP assisted with ultrasonic and nanoprecipitation. The size distribution and crystalline structure of the CSNP were investigated. Interfacial properties of the CSNF at the interface of O/W system were investigated at different concentrations and temperatures. The efficiency of electrolyte and ultrasonic interaction was also determined. The efficiency of CSNF in altering wettability of sandstone as a function CSNP concentration, salinity and temperature was investigated. A core flooding experiment was conducted at reservoir condition to justify the effect of wettability alteration and IFT reduction of CSNF on additional oil recovery. And the performance of the CSNF was compared to the conventional EOR chemical.

Materials and methods

Materials

Cassava tubers were purchased from Monday Market at Taman Teratai, Johor Bahru, Malaysia. Pineapple fruits and oranges were purchased from Monday Market at Taman Teratai, Johor Bahru, Malaysia. Lemongrass was harvested at Universiti Teknologi Malaysia (UTM) campus. Palm wine with a purity of 94% used in place of alcohol and surfactant was obtained from Kangkar Pulai, Johor. Xanthan gum was supplied by R & M Marketing, Essex, U.K. Sodium chloride (NaCl) used in the preparation of the different brine solution was supplied by QREC (ASIA) Sdn. Bhd., Selangor, Malaysia with molecular weight of 58.44 g/mol and a purity of 99% assay. Vinegar with molecular weight of 60.05 g/mol, acetic acid (5%) and density of 1.0446 g/cu @25 °C were supplied by PubChem. A West Lutong crude oil sample with a density of 0.8 g/mL @25 °C, API gravity of 37.7 and viscosity of 10 cp @25 °C was obtained from Sarawak oil field in Malaysia. Core samples from a sandstone formation located in Sarawak, Malaysia were used. Table 1 shows the

Table 1 Properties of core samples

Properties	Core #1	Core #2	Core #3
Length (cm)	9.7	9.8	9.9
Diameter (cm)	3.7	3.7	3.7
Bulk volume (cm^3)	104.30	105.37	106.45
Pore volume (cm^3)	16.00	16.00	16.00
Porosity (%)	15.3	15.2	15.0
Permeability (mD)	167.43	152.24	102.53
Initial oil saturation (%)	98.13	93.44	95.00
Injection rate (mL/min)	0.5	0.5	0.5

properties of the core samples. Deionized water (DIW) was used for sample preparation, whereas distilled water (DW) was used to prepare the dynamic light scattering (DLS) samples. NaCl, vinegar, crude oil and palm wine were used without further purification.

Methods

Formulation of cassava starch (CS)

Cassava tuber weighing 15 kg was peeled, washed and grated to fine particles. Starch was extracted from the grated pulp by sieving, while the fibre was retained on the sieve. The fibre retained was washed repeatedly for at least three to four times on a screen to remove the remaining starch. The extracted starch was allowed to sediment, after which it was decanted off and the starch rewashed with distilled water to remove the remaining fibre. The starch was dried in an oven at a temperature of 45 °C for about 6 h to reduce the moisture and then sun dried for 4 h. This is to bleach the starch and reduce the cyanide content. A dry weight of 3.06 kg of the sample (10–30 μm) with 75 wt% amylopectin and 25 wt% amylose was obtained. It was then passed through a 60-μm mesh size sieve (British Standard) and stored in an airtight container for analysis.

Extraction of ascorbic acid

Pineapple weighing 1.81 kg and 0.79 kg of oranges were washed with DW, and the skin removed by peeling with a sterilized knife to expose the flesh. The flesh was cut into chunks and blended to obtain 32.5 oz and 24 oz of juice, respectively. The juice was collected and sieved to get a clear solution, poured into a container and refrigerated at 4 °C. The lemongrass was hand-picked, and it was washed thoroughly with DW to remove dirt and impurities. A portion of 30 g of the washed lemongrass was weighed and transferred into 250 mL beaker containing 100 mL of distilled water and boiled for 20 min. The extract was collected and sieved through a No. 1 filter paper to remove particle matter and

get a clear solution. The solution was refrigerated at 4 °C in 250 mL Erlenmeyer flask for analysis.

CSNP production

The technique used here is the combined method of nanoprecipitation and hydrolysis assisted ultrasonic using weak acid, alkaloids and enzymes from plant extracts. 40 g of CS was dissolved in 20 mL of vinegar to form a solution. The solution was added dropwise into a fixed quantity of absolute alcohol (palm wine). The plant extract was added slowly to the solution at a ratio of 1:10 (v/v) for the bio-reduction. The mixture was stirred continuously using a magnetic stirrer at a constant stirring rate (1100 rpm) under a temperature of 60 °C for 120 h (slow hydrolysis due to weak acid used). The mixture was then placed in an ultrasonic bath (W: 21 cm×L: 50 cm×H: 30 cm). A Crest Genesis™ XG-500-6 ultrasonic generator with a frequency of 40 kHz and power output of 500 W provided the ultrasound for 1 h. The resulting mixture was then centrifuged, and the supernatant removed to obtain the regenerated nanoparticles. The nanoparticles were rinsed 3 times to remove alcohol, free surfactant, acid, vinegar and air dried.

The energy required for the synthesis process was calculated using the method of Adewuyi and Deshmane (2015) according to the following equation;

$$E = \frac{Pt}{R_m},\tag{1}$$

where E is the required energy (J/g), P is the applied power (J/s), t is the ultrasonication time and R_m is the amount of treated raw material in grammes.

Morphology

The morphology of the CS was analysed using a Zeiss (LEO) 1450VP scanning electron microscope (SEM). The sample was placed on a slide with two-sided carbon conductive tape sputter-coated with gold. The samples were viewed and photographed at an accelerating voltage of 13 kV and a magnification of 500×. The size of CSNP was determined using a Transmission Electron Microscope (TEM), (HITACHI, Model: HT 7700) 120 kV high resolution. The CSNP was dispersing in DIW and placed on a platinum-coated microscopy grid for analysis.

Particles size analysis and surface charge

The size and surface charge of the particles were measured using DLS litesizer 500 Anton Par equipment. The CSNP was dispersed in DW at a concentration of 0.1% (v/v). The sample was then transferred to the Omega cuvette for measurement. The measurement was done at 25 °C at a fixed

backscattering angle of 170°. The refractive index (RI) and the viscosity of the DIW were 1.3303 and 0.8903 mPa s, respectively.

Crystallization structure variation

The structure of the CSNP was measured using an X ray diffractometer (XRD), (Rigaku SmartLab, Japan) machine. With a CuKβ radiation (40 kV and 30 mA). The radiation was detected at 2θ angle scanning ranges of 3°–50° at 8.2551°/min. The relative crystallinity (RC) was quantitatively calculated using the method of Nara and Komiya (1983) according to the following equation:

$$RC\,(\%) = \frac{A_c}{A_a + A_c}, \tag{2}$$

where A_c is the crystalline area, and A_a is the amorphous area on the X ray diffractogram.

Nanofluid Preparation

Different concentrations of CSNF (0.05–0.2 wt%) were prepared by dispersing CSNP in DIW. The different solutions were homogenized, stirred for 3 h and ultrasonicated for 30 min as previously described, to form a stable solution. A weight of 0.2 wt% CSNF was prepared in different synthetic brine solutions (0.9–2.2 wt%). These salinity concentration ranges represent the typical Malay Basin oilfield salinity (Agi et al. 2019a, b).

IFT measurement

The IFT between DIW, CSNF and West Lutong crude oil was measured using K20 Easy Dyne Kruss tensiometer (Kruss GmbH, Germany). The ring method was used to calculate the IFT of the CSNF at different concentrations as a function of electrolyte concentrations and temperature (26–80 °C) using the method of Korenko and Simko (2010) according to the following equation:

$$\sigma = \frac{F}{4\pi R \cos\theta}(0.725 + \sqrt{\frac{9.075 \times 10^{-4}F}{\pi^3 \times \Delta\rho \times g \times R^2}}$$
$$- \frac{1.679r}{R} + 0.04534), \tag{3}$$

where σ is the IFT, F is the force acting along the 3-phase contact line which is equal to the weight of the liquid meniscus above the plane of the fluid–fluid interface, $\Delta\rho$ is the density difference, $\cos\theta$ is the surface wettability, g is the

acceleration due to gravity, R and r are the outer and inner radii of the ring, respectively.

Sample preparation and contact angle measurement

16 sandstone cores (1 cm thick × 5 cm diameter) were polished and cleaned with acetone, toluene and DIW to remove impurities. The clean substrates were air-dried for 24 h to remove any residual contaminants. The polished sandstone cores were rendered oil-wet by immersing in crude oil for 78 h at 90 °C. It was then cleaned with n-heptane to make it visible and more oil-wet. The sandstone cores were then air-dried for 24 h. Oil-wet sandstone cores were immersed in CSNF of different concentrations for 78 h and then dried for 24 h. The cores were placed vertically at an angle of 90° for wettability alteration to occur by adsorption on the surface rather than deposition. Sessile drop method was used to determine the angle of contact at 26–80 °C. The sandstone cores were held horizontally using a retort stand and a U-shaped needle was used to inject an oil droplet 0.1 cm³ on the sandstone core surface. A Nikon P900 (16.0 megapixel) microscopic digital camera captured the side image of the drop. The images of the oil drops were analyzed using Image J 1.48 s image analyzer software. Figure 1 shows the schematic diagram of the contact angle measurement.

Oil displacement test

A high-temperature high-pressure (HPHT) core flooding equipment (Fars EOR Technologies) was used to determine the performance of the xanthan and CSNF at reservoir conditions. Figure 2 shows the schematic and pictures of the core-flood equipment. The core-flooding equipment is dedicated for evaluating oil recovery for different injection fluids with a maximal pressure capacity of 6000 psi and temperature capacity of 150 °C. The apparatus is composed of fluid accumulator for brine, oil and chemicals, a back-pressure controller, core holder, a digital control oven and over-burden pressure. An ISCO displacement pump for liquid injection was used to pump liquid from the accumulator through the core-flooding system. A processor was linked to the equipment to control the flooding procedure, take pressure, temperature and flow rate readings. The distillation extraction method in a Soxhlet column containing toluene was used to clean the cores. The cores were then dried at 100 °C for 48 h. To simulate a typical Sarawak oil field reservoir, the system was vacuumed and subsequently pressurized to 3000 psi with a back pressure of 100 psi and the temperature of the oven was increased to 120 °C. The core was saturated with 1.5 pore volume (PV) of synthetic formation brine (2.2 wt%); 0.5 mL/min of crude oil was injected into the core until water production ceased and the residual oil saturation was determined. The system was then aged for

Fig. 1 Schematic diagram of contact angle measurement
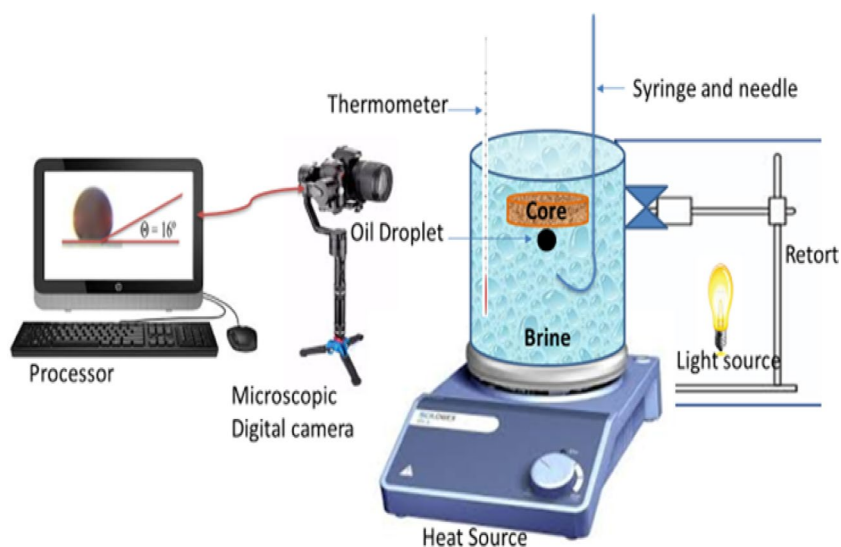
24 h to establish equilibrium between the liquid and the rock surface to attain uniformity. Water flooding was performed and sustained until oil cut was less than 1%. EOR was commenced by injection of 0.5 PV containing 0.2 wt% of CSNF or xanthan to recover the residual oil. All the experiments were conducted at reservoir temperature (120 °C) and pressure (3000 psi), except where otherwise stated.

Results and discussion

Morphological, mineral composition and structural change

The SEM photograph of the CS starch is shown in Fig. 3. The starch granules are mainly oval and spherical in shape. The surface appeared to be smooth which suggests that the method of extraction and drying did not cause any significant damage to the starch. The starch contains hollow-shaped granules (Fig. 3a); this could be because of the granular swelling and then collapse during preparation. A similar result was observed by the previous study of Chen et al. (2011) where they reported that starch granules underwent swelling followed by the collapse in a concentrated solution of compound enzymes. The granules range from 10 to 30 µm with an average size of 10 µm (Fig. 3b).

The insert (Fig. 3a) shows an inspection field within which the energy dispersive X ray (EDX) data were collected. This was done by restringing the incident electron beam to provide the spectrum shown (Fig. 3c). The result reveals that C and O are the main elements present within the inspection field of CS, with C being dominant. The EDX spectrum shows the homogeneity and the gradient of the elements present in the sample and there are no other peaks,

which confirms the purity of the samples. The C-content confirms the biological origin of the samples.

Figure 4 shows the TEM image of the CSNP and the image confirmed that the synthesis method resulted in a decrease in size of the granules, which released nano-sized particles about 6.97–200 nm. The CSNP developed platy and pear-like structures (Fig. 4a) of about 163 nm from which smaller fragments emerged. This suggests that this might be the last part of the CSNP to be modified which agrees with the previous work of Kaur et al. (2004). Also, it might be due to an aggregation of the already formed CSNP, which is consistent with the previous study of Shahrodin et al. (2015) where they observed a dense, opaque and apple-like structure during acid hydrolysis of CS.

The fragments from the eroded surface were deposited beneath showing spherical structures ranging from 10.1 to 19.1 nm. The results show that there are two hydrolysis processes involved in the synthesis: (1) a fast-moving hydrolysis of the amorphous region of the CS granules, which resulted in small size nanoparticles, and (2) the larger size nanoparticles were the result of the hydrolysis of the crystalline region which was slower (LeCorre et al. 2011). This could be because of the dense packing of the starch helixes in the crystalline region which might have prevented penetration of H_3O^+ (LeCorre et al. 2011).

Particle size analysis and surface charge

Figure 5 shows the particle size distribution of CSNP. It shows that the aggregates of the CSNP were successfully disconnected by the ultrasonic (Kim et al. 2013). The polydispersity index (PDI) value of 0.28 indicates a relatively homogenous solution. PDI values less than 0.5 indicate a relatively homogenous suspension. It reflects the width of the detected peaks (LeCorre et al. 2011). The CSNP shows a
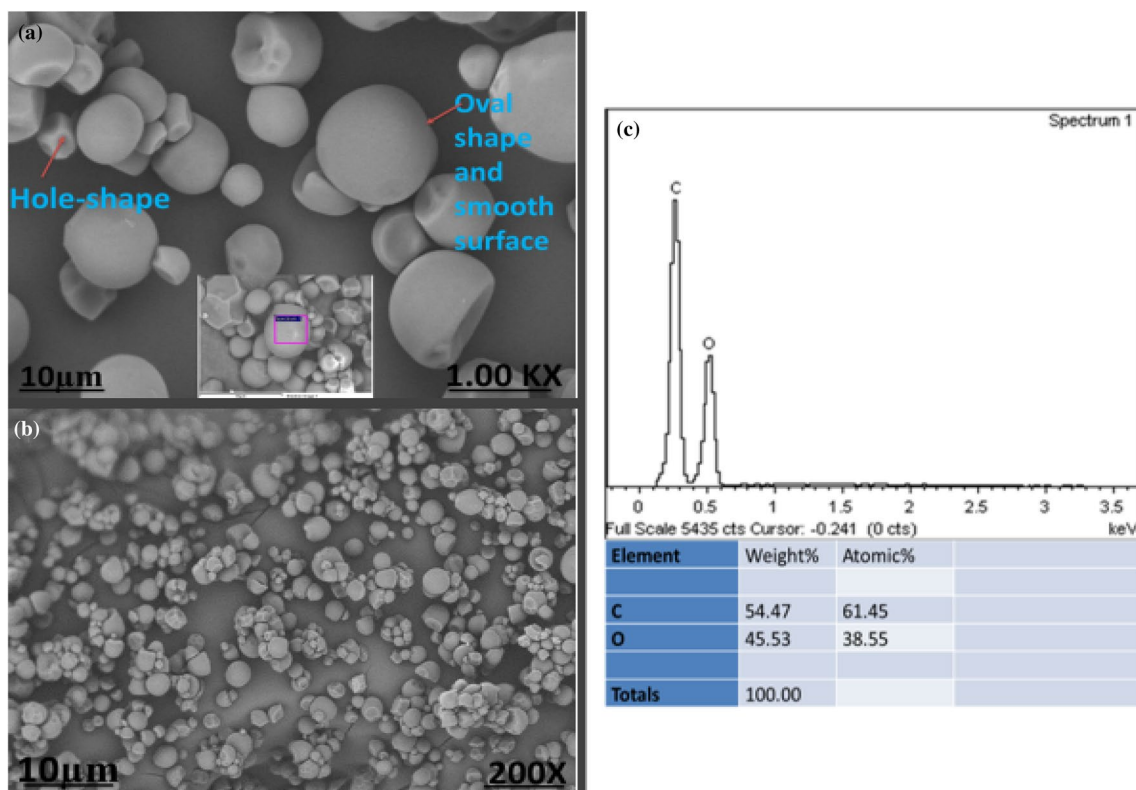
Fig. 2 **a** Schematic of the core-flooding experimental apparatus. **b** Picture of experimental setup
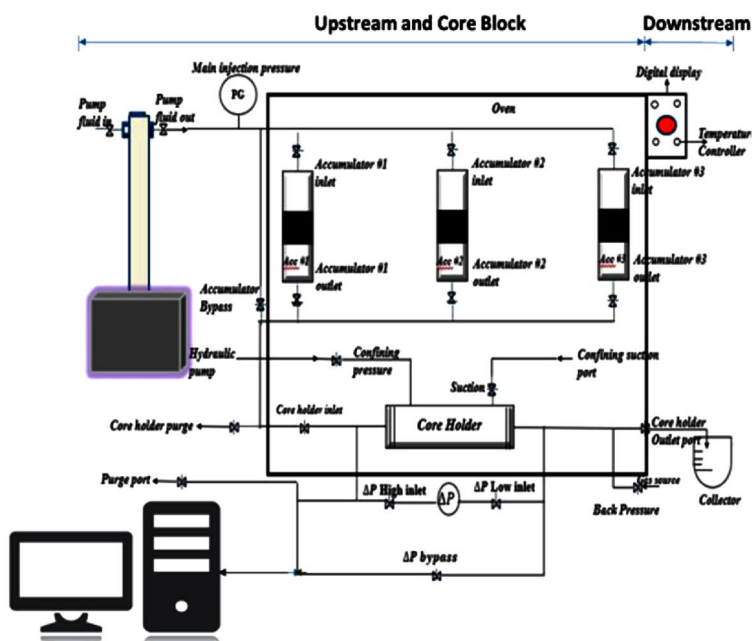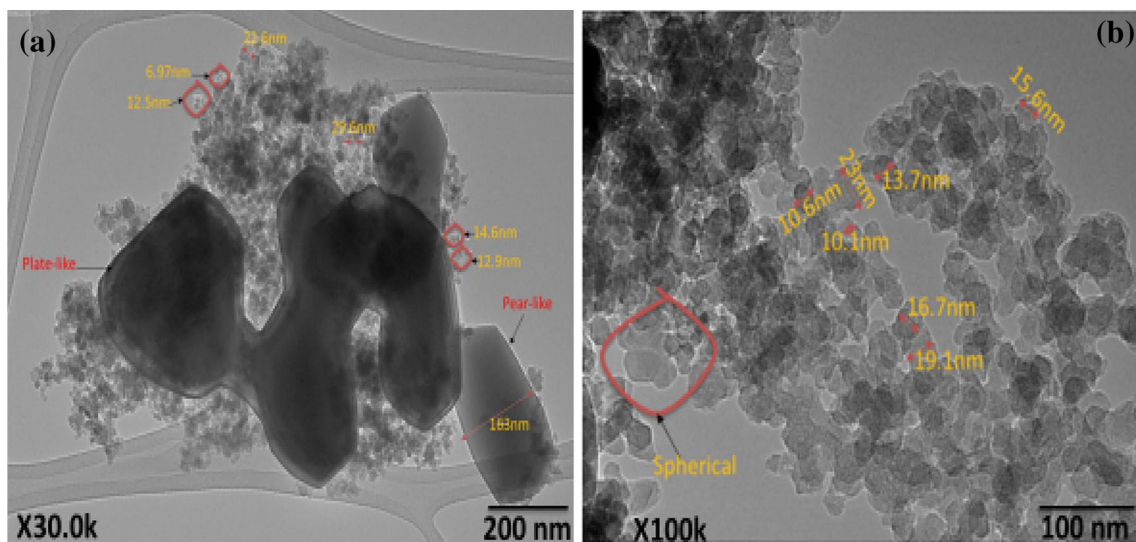

(a) Schematic of the core-flooding experimental apparatus

(b) Picture of experimental setup

Fig. 3 **a** SEM images with the insert showing the inspection field within which EDX data were collected. **b** SEM image with magnification 200×. **c** EDX spectra of CS
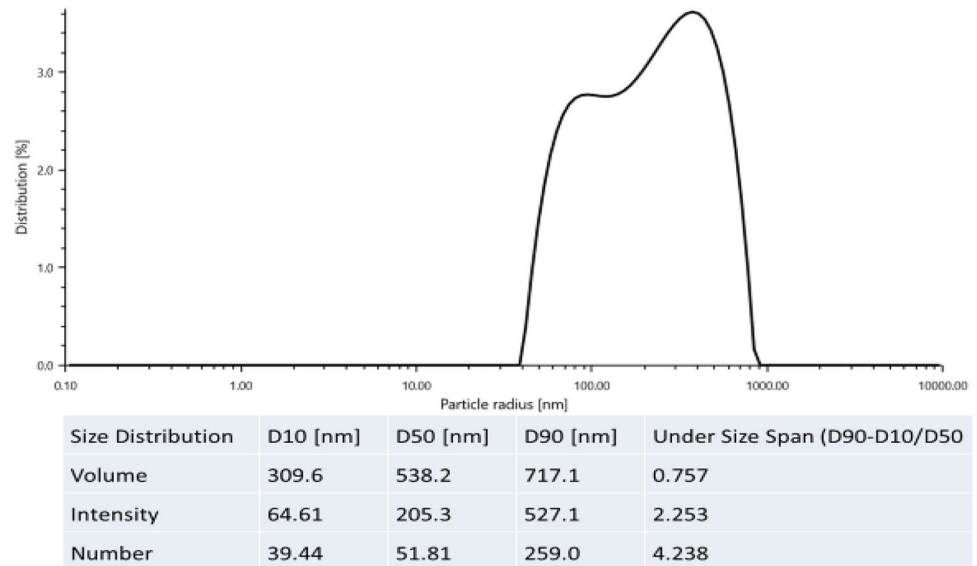

Fig. 4 TEM image of CS nanoparticles **a** showing plate-like shape, **b** showing spherical shape

bimodal distribution with a mean diameter (D_{50}) of approximately 538.2 nm. This shows that the CSNP consists of different sizes which is consistent with TEM result (Fig. 4), but it shows larger nanoparticle sizes compared to the TEM result. This is because DLS measures the hydrodynamic size

(Zetasizer Nano Series 2015). Therefore, the diameter calculated is only representing the superficial size of the hydrated particles. It does not replicate the exact size of the non-monodispersed and non-spherical samples. Hence, even with the fractionation, the measurement remains complicated

Fig. 5 Particle size distribution by intensity of CSNP

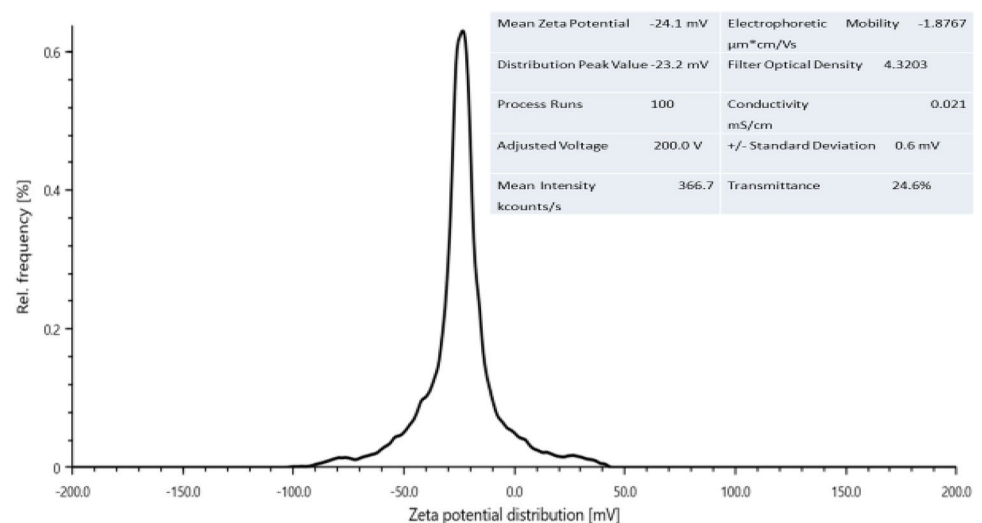| Size Distribution	D10 [nm]	D50 [nm]	D90 [nm]	Under Size Span (D90-D10/D50
Volume	309.6	538.2	717.1	0.757
Intensity	64.61	205.3	527.1	2.253
Number	39.44	51.81	259.0	4.238

(LeCorre et al. 2011). Therefore, the stated hydrodynamic diameter cannot be used as an estimate of size but for comparison (LeCorre et al. 2011).

The CSNP exhibited a mean zeta potential of − 24.1 mV (Fig. 6) which lies in the stable zone range, indicating that the CSNP system is stable. The negative charge indicates that the CSNP surface is negatively charged. This could be attributed to microfuidization of the CSNP, which increased the zeta potential resulting in the more negative charge. This indicates that homogenization-induced conformational changes increase the number of charged groups on the CSNP hydration surface (Huang et al. 2012). The result implies that the hydrolysis and ultrasonic process were enough to reduce the CS to nanoparticles, which gave it a good stability in the form of suspension. This resulted in the moderate mean surface charge due to a favourable particle–particle interaction. Furthermore, during hydrolysis, starch is vulnerable to superficial esterification. The OH group is replaced by the $-OSO_3^-$ group creating an electrostatic repulsion caused by the valence electron (Huang et al. 2012). The presence of these negative charged group on the surface of the CSNP tends to increase the zeta potential (Huang et al. 2012). The repulsion among the CSNP with the same type of surface charge provided the extra stability. After ultrasonic treatment, CSNP was produced in the form of a colloidal liquid suspension. The results show that there exists a correlation between the PDI, zeta potential and size of the particles. Increase in zeta potential can enhance the electrostatic force, kerb aggregation and reduce the hydrodynamic diameter.

Fig. 6 Zeta potential distribution of CSNP

Mean Zeta Potential	-24.1 mV	Electrophoretic Mobility	-1.8767 μm*cm/Vs
Distribution Peak Value	-23.2 mV	Filter Optical Density	4.3203
Process Runs	100	Conductivity mS/cm	0.021
Adjusted Voltage	200.0 V	+/- Standard Deviation	0.6 mV
Mean Intensity kcounts/s	366.7	Transmittance	24.6%

Crystallization structure variation

Figure 7 shows the XRD diffraction of CS and CSNP. The occurrence of peak at $2\theta = 15.1°$, $17.1°$, $23°$ and $29.5°$ shows that the CS is a C pattern. It was observed that the CS shows few straight peaks of both A crystallinity ($2\theta = 15.1°$) and B crystallinity ($2\theta = 17.1°$, $23°$ and $29.5°$), and characteristics of a type C crystallinity. Starches are classified as type A, B or C based on the kind of crystalline structure in the granules. In a type A starch, the double helices of the chain are densely packed, whereas in a type B crystal with a pseudohexagonal system they are formed by rather loosely arranged double helices. But both polymorphs are identical. Type C is a blend of A and B. Type A is mostly shown by cereals, whereas the type B pattern represents the factual crystalline form of CS. Type C is believed to be the superposition of A and B. The complete disappearance of the peak indicates that the CS has been changed into non-crystalline states. The broad spectrum and featureless peak are attributed to amorphism. CSNP shows similar peaks with CS at $2\theta = 15.1°$, $17.1°$, $23°$, but higher diffraction intensities were observed, and the crystalline peaks became higher compared to CS (Huang et al. 2012). This is because the amorphous area of the CS was hydrolysed more extensively than the crystalline. Amylolysis occurs in the amorphous area of CS. Increase in intensity of CSNP is due to the weak-acid hydrolysis of the non-crystalline domain. Weak-acid penetrated the CS granule cavities and channels which might have disrupted the amorphous phase and increased the crystalline peak. The disappearance of the peak at $2\theta = 29.5$ shows a reduction in the type B crystallinity. The loss of the B-type peaks and the appearance of A-type peaks show that CS changes from C to A-type pattern. The B-type polymorph in the C-type CS is degraded quicker compared to the A-type polymorph in the weak-acid hydrolysis. That is, the amorphous area was hydrolysed before the crystalline region and the B-type polymorph in the C-type constitutes the amorphous region, whereas the crystalline regions are made of the A type polymorph. Also, the disappearance might be
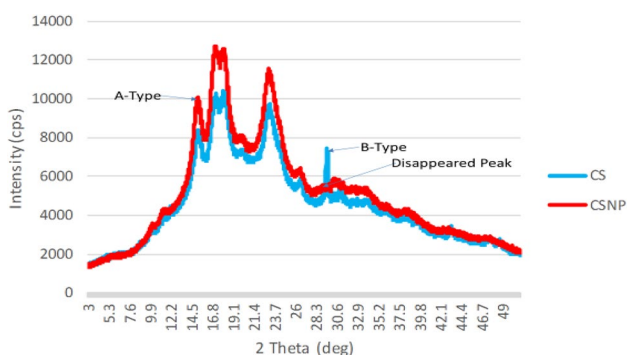
attributed to the ultrasonication process which might have influenced the structure of the CSNP, which might be credited to the excessive reduction in the size of the particles. This is because the intensities produced by small crystals might be too small to be measured, especially for an element such as carbon. This is due to the fact that the deflection of carbon is proportionate to the square of the atomic number.

The RC of the CSNP is 23% compared to 16% of CS; this is consistent with existing literature. Native starch contains between 15 and 45% of crystallinity depending on their botanical sources (LeCorre et al. 2011). The increase in RC of CSNP is because the amorphous region of the CS was removed by the weak-acid hydrolysis. The starch chain present in the amorphous region cleaves together concurrently, rearranging the chain segment to a better structure. The higher RC can also be linked to the hemicellulose and lignin removal from the CS, which exist in the amorphous region during weak-acid hydrolysis. The precipitating medium preserved the crystallinity (23%); this is because of the formation of a helical structure as the alcohol was added resulting in higher crystallinity (Qin et al. 2016). The CSNP was precipitated by the addition of alcohol. The ratio of alcohol used might have also affected the morphology of CSNP. It also contributed to retaining the crystallinity of the CSNP. The increase could also be a result of high amylose content of the CS which agrees with the previous study of Qin et al. (2016). Preservation of RC by the precipitating medium shows the preservation of a strong connection of the molecules, a higher level of interaction between the CSNP bond and higher perfection of the crystal lattice.
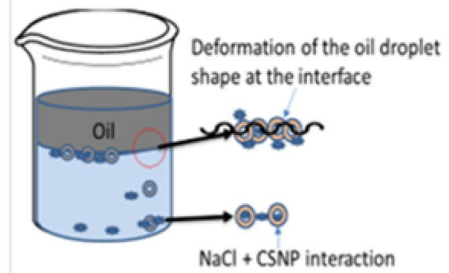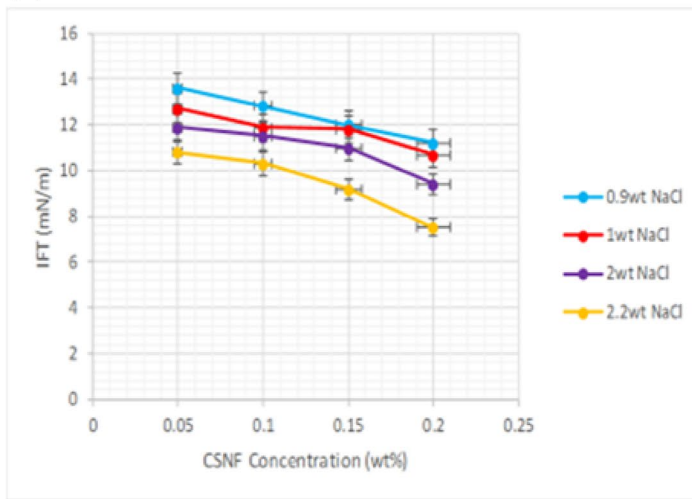
Effect of concentration on IFT of CSNF

Figure 8a shows the effect of change in concentrations (0.05–0.2 wt% w/v) on the IFT of CSNF. The result shows the dependence of O/W IFT on CSNF concentration. IFT decreased with the increase in concentration of the CSNF, which is consistent with the studies of Pei et al. (2017), Ogunlaja et al. (2017), and Ye et al. (2017). As the concentration of the CSNP increases, more particles are driven to the O/W interface. This phenomenon increases the migration of surface-active agents from the bulk solution to the interface, subsequently promoting the adsorption of the CSNF at the interface and the propensity of the surface-active agents (long chain of the CSNF) to accumulate at the O/W interface forming a layered structure (Yekeen et al. 2019). This layer increases the potential between the particles and imparts a repulsive force between them, which reduced the energy at the interface and IFT. The repulsive force was induced by an acid group of CSNF that polarised the water, whereas the thioglycolic group of the CSNF induced an electrostatic interaction that synergistically reduced the IFT. Therefore, on increasing the CSNP concentration, this
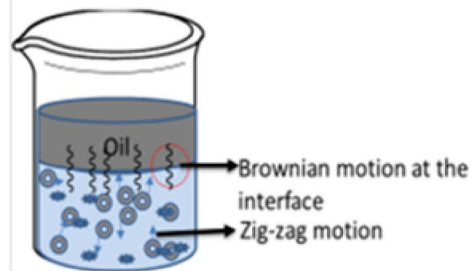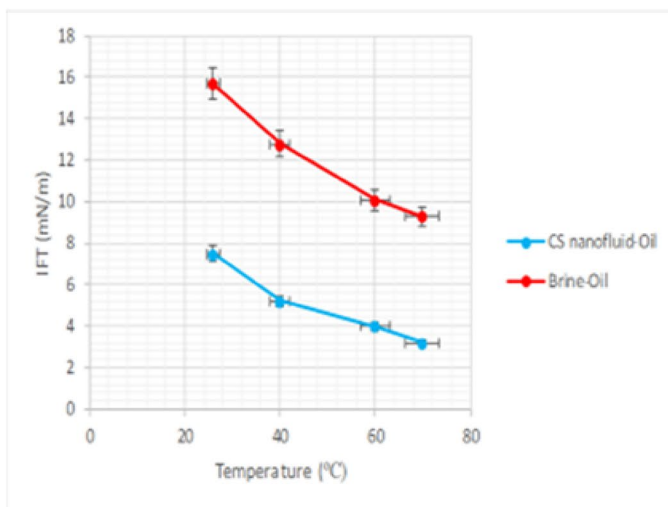

Fig. 7 XRD diffraction pattern of CS and CSNP

(a)
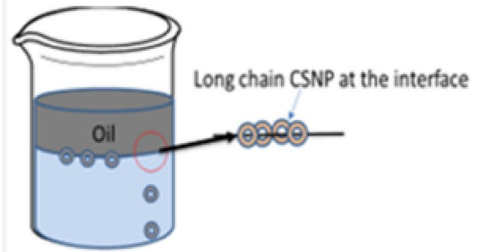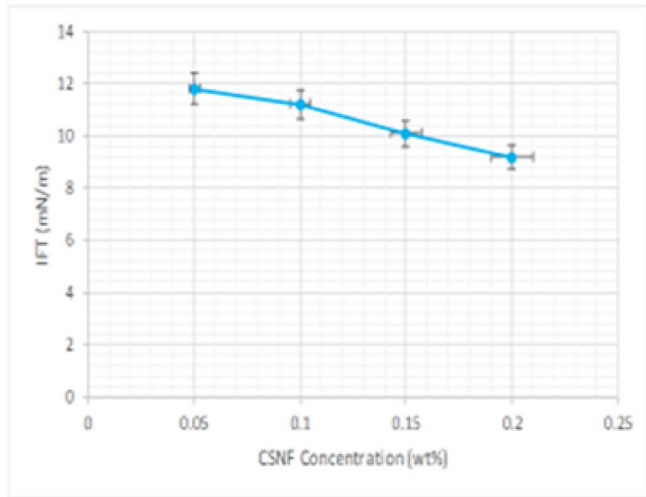
(b)

(c)

◀**Fig. 8 a** IFT of CSNF (DIW) as a function of concentration, show-ing the proposed mechanism of IFT reduction. **b** Influence of elec-trolyte on IFT as a function of CSNF concentration, showing the mechanisms of IFT reduction in the presence of electrolyte. **c** IFT of CSNF (DIW) and electrolyte as a function of temperature, showing the mechanism of IFT reduction

mechanism became more effective and stronger (Ali et al. 2019). Increase in concentration increased the interfacial area and reduced the energy at the interface which might have also reduced the IFT. This is because the ultrasonic reduced the surface area to volume ratio and increased the hydrophobicity of the CSNF. This is inline with the study of O'Sullivan et al. (2016) who reported that ultrasonic stimulation makes the interfacial film more hydrophpbic. This enables the sonicated aggregate to absorb faster to the interface forming an electrostatic film, inducing steric and electrostatic interraction and thereby reducing IFT. This is because at high ultrasonic wave, compression and expansion enact stress to the interface overcoming the interconnected force that holds large droplet breaking them to smaller ones. This increases outward motion and the hydrophobicity at the interface, resulting in an increased cavitational threshold. The cavitational threshold decreases cavitational activity and thus the amplitude of the interfacial instability is reduced (Gaikwad and Pandit 2008).

Influence of electrolyte concentration on IFT of CSNF

The IFT of crude oil and nanoparticles with NaCl (0.9–2.2 wt%) is shown in Fig. 8b. The IFT decreased with increase in NaCl concentration. This might be due to the dis-solution of the crude oil compound by NaCl and subsequent sorption of the amphiphilic compound at the interface of O/W. This liquified crude oil in the NaCl acted as a natural ionic and non-ionic hydrocarbon surfactant (Ghorbanizadeh and Rostami 2017). It might also be because of the syner-getic influence of the NaCl and CSNP on the IFT. The NaCl lowered the solubility of the CSNP making it less ionized, which might have resulted in the CSNP adsorption on the O/W interface. The effect of ultrasonic was also felt in the aqueous suspension containing NaCl and CSNP to which the sonication was applied, as the NaCl produced dilute aque-ous dispersion of the CSNP that deformed the shape of the oil droplet at the interface which might have reduced the IFT. Ultrasonic increased the concentration of the surface-active agent formed by the addition of NaCl which led to phase separation and decreased volume fraction of the chi-ral nematic and isotropic phase. Ultrasonic also hindered the formation of anisotropic phase formation in the CSNP suspension and influenced the formation of a double elec-trode layer and reduced the layer at the interface (Beck et al.

2011), which led to the CSNP molecules arranging them-selves at the interface which increased the surface activity of the polar impurities. In the presence of NaCl, the impurities are salted out and concentration at the O/W interface lowers the IFT (Bera et al. 2014).

Temperature effect on the IFT of CSNF

The effect of temperature (26–80 °C) on the IFT of CSNF at the same concentration (0.2 wt% w/v) was investigated and is shown in Fig. 8c. The results show that CSNF reduced the IFT by 52% compared to brine (NaCl 0.2 wt%) at 26 °C, which shows that IFT of the CSNF decreases with increase in temperature. This is because the increase in temperature of the CSNF increases the kinetic energy of the liquid mol-ecules. During the ultrasonication of the CSNF, cavitation played a vital role in percolation of phases exposed to ultra-sound. CSNF molecules tend to migrate to the interface and coalescence occurs. The coalescence of the CSNF droplet is because of collision frequency of dispersed nanofluid, acous-tic streaming, the attractive force acting between the oscillat-ing droplet and heat generated during sonication (Bjerknes forces), which led to expansion and weakening of the inter-molecular forces at the interface during the IFT test, thereby reducing IFT. At higher temperatures there is an increase in the zig-zag motion of the particles (Brownian motion). The Brownian motion builds inside the molecule of the liquid; this will in turn reduce the interconnected energy and the IFT of the system (Murshed et al. 2008). It might also be due to an increase in solubility of O/W; the increase in solubility decreases the interfacial energy which lowers the IFT.

Influence of CSNF on wettability alteration

The influence CSNF on the wettability of the sandstone core through the contact angle method was investigated. The contact angle can determine the wettability of a rock. A rock can be water-wet if the $\theta < 70º$, intermediate wet if $70 < \theta < 110°$ or oil-wet if $\theta > 110°$. Figure 9i shows the con-tact angle CSNF-modified sandstone core versus nanofluid concentration. The contact angle decreased as the concentra-tion of the nanofluid increased. The result reveals that CSNF changed the wettability of the sandstone cores from oil-wet to water-wet. The oil droplet at 26 °C reveals that the refer-ence angle of the sandstone cores is 117° (Fig. 9ii a) which indicates an oil-wet wettability. The wettability was altered in the presence of CSNF to water-wet (Fig. 8ii b–d). This could be because of the adsorption of CSNP on the surface of the sandstone core that enhanced the wettability of the oil-wet sandstone to water-wet condition.

The CSNF then spread on the surface forming a wedge-film on the surface (Fig. 9iii), resulting in an ordered struc-ture. This is consistent with the previous study of Kondiparty
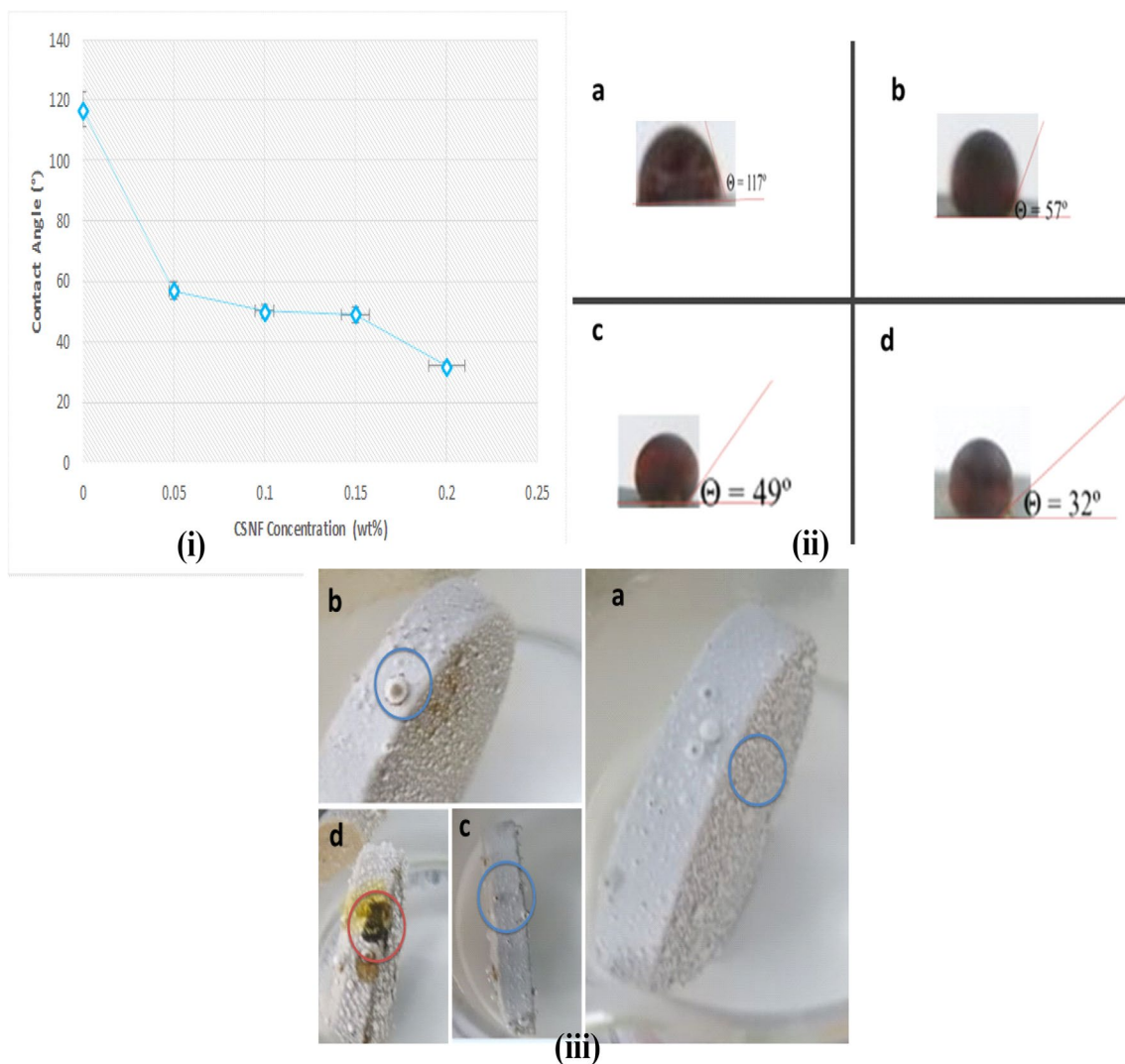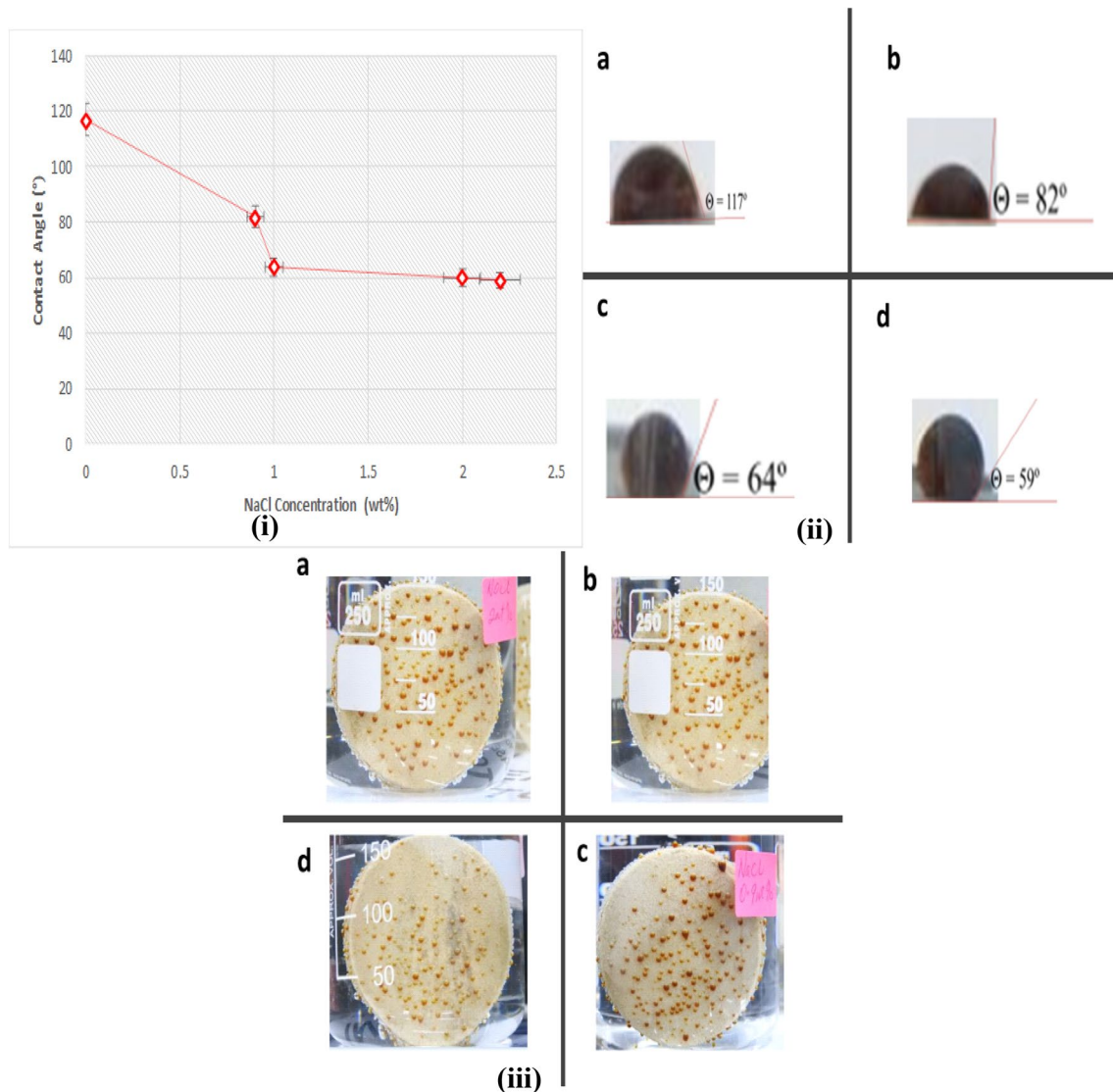
Fig. 9 i Oil contact angle on CSNF-modified sandstone surface as a function of nanofluid concentration. **ii** Microscopic image of oil droplets (flipped image) (a) without nanofluid, (b) in the presence of 0.05 wt% nanofluid, (c) 0.15 wt% nanofluid, (d) 0.2 wt% nanofluid (**iii**, a–c) Formation of wedge-film on the surface of sandstone core by CSNF (d) shows oil removal by CSNF

et al. (2012) where they observed that in a three-phase contact region (oil-solid-aqueous), particles tend to form wedge-film at the discontinuous phase and substrate (structural disjoining pressure), which is at the contact line between the oil and the sandstone rock (Fig. 9iii d). This structural disjoining pressure is caused by Brownian motion and the electrostatic repulsion between the CSNP during ultrasonication (Kondiparty et al. 2012). As nanoparticles tend to arrange themselves in a well-ordered layer when confined in a thin layer as observed in Fig. 9iii, there is a correlation between the disjoining pressure and the ability of the CSNF to spread on the surface, which is due to the imbalance between the interfacial forces at the three-phase region. The magnitude of spreading and the disjoining pressure could be influenced by the PDI and particle charge on the nanoparticles.

CSNP–electrolyte interaction on wettability alteration

Electrolyte concentration can influence the flow behaviour of nanofluid. The effcet of NaCl concentration (0.9–2.2 wt%) on CSNF (0.2 wt%) was investigated. Figure 10i shows that increase in NaCl concentration decreased the contact angle from 117–59 degrees. This could be because of the negative surface of the CSNF which created an electrostatic repulsive force that prevented agglomeration and sedimentation (Zargartalebi et al. 2015). This shows that the CSNF is still stable when interacting with electrolyte, which is consistent with the zeta potential results (Fig. 6) which controlled the surface charge.

Fig. 10 **i** Oil contact angle on CSNF-modified sandstone surface as a function of NaCl concentration. **ii** Microscopic image of oil droplets (flipped image) (a) without nanofluid and brine (b) in the presence of 0.9 wt % NaCl (c) 1 wt% NaCl (d) 2.2 wt% NaCl. **iii** Oil removal from sandstone core due to reactivity

The oil droplet image (Fig. 10ii) shows that CSNF can still alter the wettability of the sandstone core in the presence of an electrolyte. The electrolyte awakened the repulsive force between the CSNP and accelerated the precipitation of the CSNF when in contact with the sandstone. This resulted in the oil surface being more negatively charged due to electrostatic repulsion at the 3-phase contact forming a contact line. As the contact line retreated, the contact angle also decreased slowly which might have altered the wettability.

The addition of NaCl caused reactivity towards the surface of the sandstone core (Fig. 10iii). This phenomenon depends on the chemical reaction in the double layer near the surface, which resulted in physicochemical interaction or electrostatic force between the CSNF and the sandstone which led to the removal of oil from the sandstone cores as seen in Fig. 9iii d. The change in the wettability was caused by alteration which occurred at the rock/brine interface rather than at the oil/water (O/W) interface.

Effect of temperature on wettability alteration

Temperature is known to influence the wettability (Al-Anssari et al. 2017). Therefore, the effect of temperature (26–80 °C) on the change in the wettability of CSNF (0.2 wt%) in the presence of an electrolyte (2.2 wt%) was investigated (Fig. 11i). It was observed that the contact angle decreased with increase in temperature. Temperature
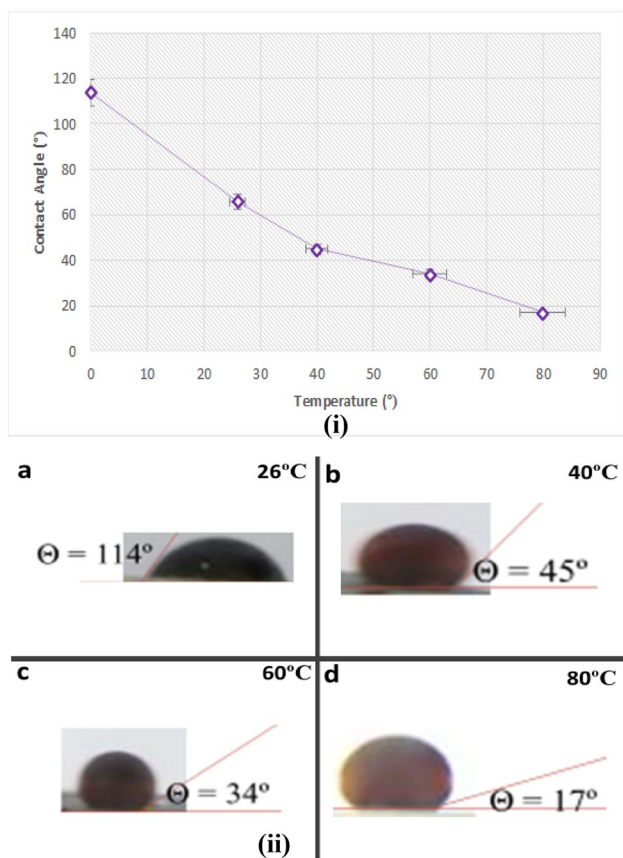
Fig. 11 i Contact angle of oil–water on sandstone surface as a function of temperature. **ii** Microscopic image of oil droplet (flipped image) (a) without treatment (reference), (b) in the presence of brine and nanoparticles at 40 °C, (c) in the presence of brine and nanoparticles at 60 °C, (d) in the presence of brine and nanoparticles at 80 °C

influences the spreading behaviour of oil drop. This is due to the decrease in active ions on the surface of the sandstone as the temperature increases (Al-Anssari et al. 2017). This enables more nanoparticles to be adsorbed on the surface of the sandstone (Fig. 9iii a) as the temperature increases. The decrease in the contact angle from 114° (reference at 26 °C) to 17° at 80 °C (Fig. 11ii) shows that CSNF is effective in altering work wettability at high temperature. This agrees with the study of Strand et al. (2006) where they reported that the spreading of the nanoparticle's font increases with the increase in temperature. Temperature breaks the hydrogen bond and the water molecules desolvated the CSNP which increases the affinity of the sandstone surface towards the CSNP.

Oil displacement results

The performance of the CSNF was determined by laboratory scale core flooding. The results were compared with commercial polymer xanthan already in use in EOR and

shown in Fig. 12i. The oil recovery after water flooding was 48% original oil in pace (OOIP); this shows that substantial amount of oil remained in the core. Tertiary recovery commenced immediately; it was observed that the oil recovery using CSNF increased by 23% OOIP compared to the initial 11% with commercial polymer xanthan. The oil recovered by the CSNF is higher compared to the xanthan; this is because the CSNF recovered the oil from very small pores by blocking the permeable zones (Kumar and Mandal 2018). The trapped oil droplets or ganglions are mobilized due to the reduction in the contact angle at the 3-phase contact. It might also be due to the enhancement of the viscosity by the CSNF which might have controlled the mobility of the displacing fluid, thereby improving the recovery by forming an oil bank. It can, therefore, be concluded that the CSNF was effective in improving residual oil recovery and the recovery was not affected by the high temperature (120 °C) and pressure (3000 psi) reservoir condition, which is consistent with the wettability results, as the wettability of the CSNF decreased with the increase in temperature. This confirms the role of wettability to recover residual oil.

The results show a positive correlation between the CSNF oil recovery and the pressure profile (Fig. 12ii). There was a sharp increase in production and pressure drop as the CSNF was injected. Production increased with pressure drop as the CSNF was injected. The rise in the pressure drop suggests that the injected CSNF interacted with the trapped oil which resulted in the dispersal of the oil into the aqueous phase and subsequent displacement from the core. The pressure drop increase was high which could be attributed to the strong oil mobilization and the two-phase flow in the porous media. The high pressure drop also demonstrates that the CSNF was more stable at 120 °C by maintaining the pressure drop during the flooding at high temperature. This shows that at 120 °C, the oil bank formation was enough to increase the oil recovery.

The high peak value of the pressure drops resulted in high oil recovery. The built-up pressure is due to the penetration of the CSNF into the remaining oil drops to form a high viscous O/W emulsion (Fig. 12iii a, d), which might have blocked the permeable water channel and reduced the movement of the oil phase resulting in improved sweep efficiency (Pei et al. 2013). This is evident in the fluctuation in the trend of the pressure drop observed during CSNF flooding as the emulsion formed can reduce the flow capacity of some channel formed during water flooding through the pore blockage mechanism and divert the injected font as well as a favourable mobility of the emulsion to displace oil banks. The formation of the emulsion during CSNF flooding is consistent with the formation of wedge-shaped film at the contact line of water/oil/rock system during the treatment of the sandstone core with CSNF during the wettability test (Fig. 9iii a–c). This phenomenon might have enhanced the
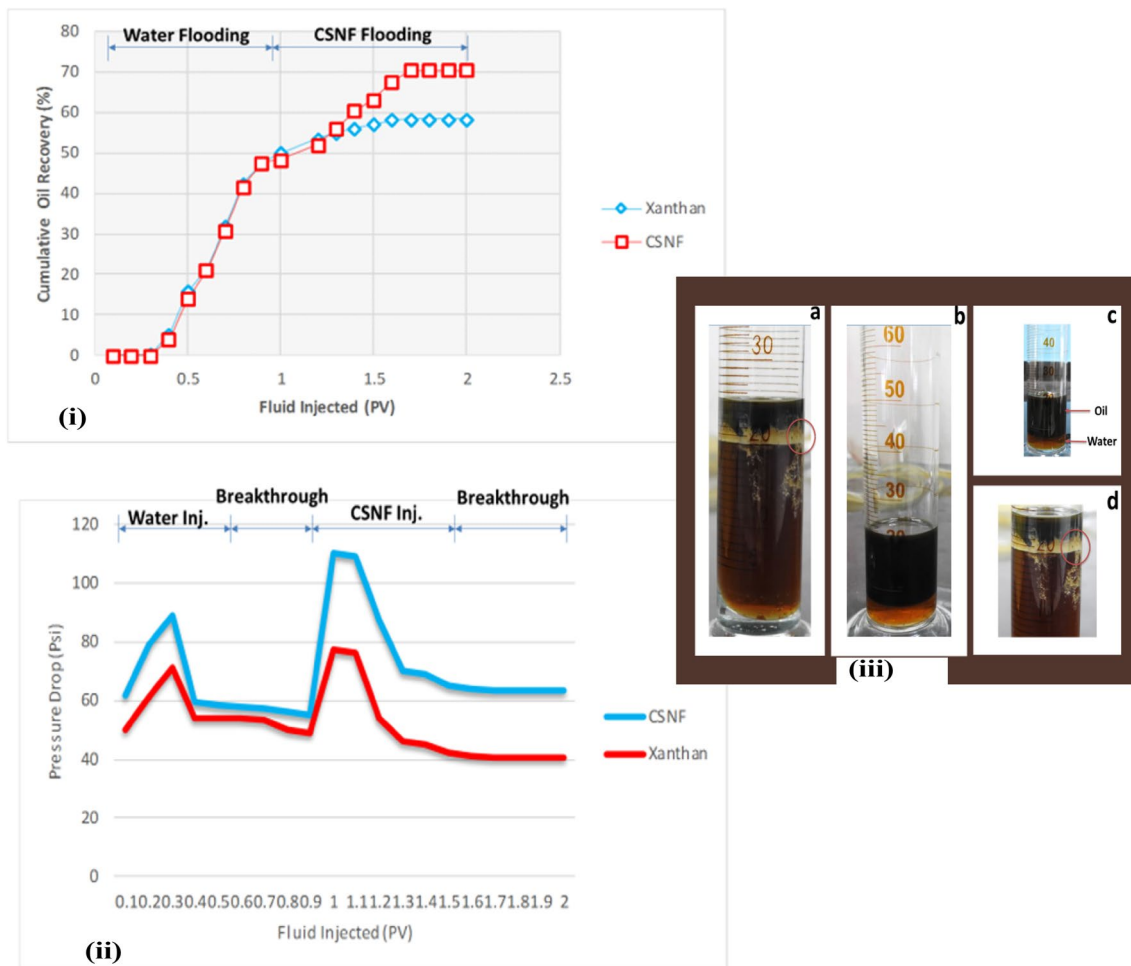
Fig. 12 i Cumulative oil production performance of CSNF, ii pressure drop profile of CSNF as a function fluid injected (iii a, d) CSNF oil recovery showing emulsion formation (b, c) Xanthan oil recovery absent of emulsion

mobilization of the oil, as the film separated the oil from the formation rock and more oil was removed (Fig. 12iii a, d) compared to xanthan flooding where emulsion formation was not experienced (Fig. 12iii b, c). Therefore, the emulsion formed under this condition improved the sweep efficiency by reducing viscous fingering and water channelling (Saha et al. 2018).

Energy and cost estimation

The energy calculated for this study was 3×10^4 J/g which is lower than the energy requirement for the steam explosion (9.90×10^4), ultrasonic-assisted enzymic hydrolysis (4.16×10^4) and other conventional methods (Adewuyi and Deshmane 2015; Velmurugan and Muthukumar 2012). This is consistent with the previous study of Nitayavardhana et al. (2010) who reported that the cost of energy consumption for ultrasonic pre-treatment of cassava chips to produce ethanol was 11 kJ compared to 22 kJ for heat treatment, which agrees

with previous studies of Bubalo et al. (2013) and Mullick and Neogi (2018) where they reported that ultrasonic provides an easy route to synthesize composite in less time and reduce energy consumption by more than 45–65% and 96%, respectively, compared to using conventional methods. Considering the capital and operating cost, a model plant would save approximately $1,114,447 each year on pre-treatment cost if it invests in ultrasonic (Montalbo-Lomboy et al. 2011). This is consistent with previous study of Chipurici et al. (2019) when they reported that ultrasonic probe system is more energy efficient compared to microwave reactor. The results show that ultrasonic vibration has a positive effect in reducing process energy consumption and the energy saving can reach as high as 85% (Jiang et al. 2019). With the low energy consumption, low cost of capital and operating cost and the use of low-cost material such as starch (US$ 0.25/kg), oranges (US$ 0.56/kg), pineapple (US$ 0.75/kg) and palm wine (US$ 0.1/l):, this method can be seen as a green and cost-effective compared to conventional methods.

Conclusions

CSNF is a potential material for EOR and can be used as an alternative to recover oil from harsh reservoir condition where application of conventional techniques has proved difficult. From the experimental results it can be concluded that the zeta potential result shows that CSNF is stable and the surface charge signifies long-term stability of the fluid when injected into oil field reservoirs. IFT decreased with increase in concentration of CSNF, electrolyte and temperature. The oil removal by CSNF was attained at low concentration and was still very effective at high-salinity concentration. The adsorption of the CSNP on the surface of the sandstone was the major mechanism that enhanced the change in wettability. And the magnitude of adsorption, spreading and structural disjoining pressure was influenced by PDI and the particle charge. CSNF changed the wettability of the sandstone surface even at very low concentration in the presence of electrolyte. And increase in temperature allowed more adsorption of nanoparticles to the sandstone surface. The pressure drops data show stability of CSNF at 120 °C and the formation of oil bank was enough to increase the oil recovery by 23%. CSNF was found to be very effective in mobilizing residual oil at HTHP reservoir condition. It can, therefore, be concluded from this experiment work that the method applied herein is easier, cost-effective and can reduce energy consumption making the method economically advantageous compared to conventional methods.

Compliance with ethical standards

Conflict of interest The authors declare that they have no conflict of interest

References

Adewuyi YG, Deshmane V (2015) Intensification of enzymatic hydrolysis of cellulose using high-frequency ultrasound: an investigation of the effects of process parameters on glucose yield. Energy Fuels 29:4998–5006

Agi A, Junin R, Gbonhinbor J, Onyekonwu M (2018a) Natural polymer flow behaviour in porous media for enhanced oil recovery applications: a review. J Petrol Explor Prod Technol. https://doi.org/10.1007/s13202-018-0434-7

Agi A, Junin R, Gbadamosi A (2018b) Mechanism governing nanoparticles flow behaviour in porous media: insight for enhanced oil recovery applications. Int Nano Lett 8(2):49–77

Agi A, Junin R, Shirazi M, Gbadamosi A, Yekeen N (2019a) Comparative study of ultrasound assisted surfactant and water flooding. J King Saud Univ Eng Sci 31(3):296–303

Agi A, Junin J, Alqatta AY, Gbadamosi A, Yahya A, Abbas A (2019b) Ultrasonic assisted ultrafiltration process for emulsification of oil field produced water treatment. Ultrason Sonochem 51:214–222

Al-Anssari S, Wang S, Barifcani A, Lebedev M, Iglauer S (2017) Effect of temperature and SiO_2 size on wettability alteration of oil-wet calcite. Fuel 206:34–42

Ali J, Kolo K, Manshad A, Stephen K, Keshavarz A (2019) Modification of LoSal water performance in reducing interfacial tension using green ZnO/SiO_2 nanocomposite coated by xanthan. Appl Nanosci 9(3):397–409

Bayat A, Junin R, Samsuri A, Piroozian A, Hokmabadi M (2014) Impact of metal oxide nanoparticles on enhanced oil recovery from limestone media at several temperatures. Energy Fuel 28(10):6255–6266

Beck S, Bouchard J, Berry R (2011) Controlling the reflection wavelength of iridescent solid films of nanocrystalline cellulose. Biomacromolecules 12:167–172

Bera A, Mandal A, Guha B (2014) Synergic effect of surfactant and salt mixture on interfacial tension reduction between crude oil and water in enhanced oil recovery. J Chem Eng Data 59(1):89–96

Bubalo MC, Sabotin I, Rados I, Valentincic J, Bosiljkov T, Brncic M, Znidarsic-Plazl P (2013) A comparative study of ultrasound, microwave, and microreactor-assisted imidazolium-based ionic liquid synthesis. Green Process Synth 2:579–590

Chen Y, Huang S, Tang Z, Chen X, Zhang Z (2011) Structural changes of cassava starch granules hydrolysed by a mixture of a & α-amylase and glucoamylase. Carbohyd Polym 85:272–275

Chipurici P, Vlaicu A, Calinescu I, Vinatoru M, Vasilescu M, Ignat ND, Mason TJ (2019) Ultrasonic, hydrodynamic and microwave biodiesel synthesis—a comparative study for continuous process. Ultrason Sonochem 57:38–47

Dufresne A (2008) Cellulose-based composites and nanocomposites. Monom Polym Compos Renew Res 2008:401–418

Gaikwad S, Pandit A (2008) Ultrasound emulsification: effect of ultrasound and physiochemical properties on dispersed phase volume and droplet size. Ultrason Sonochem 15:554–563

Ghorbanizadeh S, Rostami B (2017) Surface and interfacial tension behaviour of saltwater containing dissolved amphiphilic compounds of crude oil: the role of single-salt ionic composition. Energy Fuel 31(9):9117–9124

Giraldo J, Benjumea P, Lopera S, Cortes F, Ruiz M (2013) Wettability alteration of sandstone cores by alumina based nanofluids. Energy Fuels 27:3659–3665

Huang P, Wu M, Kuga S, Wang D, Wu D, Huang Y (2012) One-step dispersion of cellulose nanofibres by mechanical esterification in an organic solvent. Chemsuschem 5(12):2319–2322

Jiang C, Wu C, Ye H, Cheng J, Hao Y (2019) Estimation of energy and time savings in optical glass manufacturing when using ultrasonic vibration-assisted grinding. Int J Precis Eng Manuf Green Technol 6(1):1–9

Kaur L, Singh N, Singh J (2004) Factors influencing the properties of hydroxypropylated potatoes starch. Carbohyd Polym 55:211–223

Kim H, Park D, Kim J, Lim S (2013) Preparation of crystalline starch nanoparticles using cold acid hydrolysis and ultrasonication. Carbohyd Polym 98:295–301

Kondiparty K, Alex D, Darsh W, Liu K (2012) Dynamic spreading of nanofluid on solids. Part 1: Experimental. Langmuir 28(41):14618–14623

Korenko M, Simko F (2010) Measurement of interfacial tension in liquid-liquid high temperature systems. J Chem Eng Data 55:4561–4573

Kumar N, Mandal A (2018) Surfactant stabilized oil-in-water nanoemulsion: stability, interfacial tension and rheology study for enhanced oil recovery application. Energy Fuels 32(6):6452–6466

LeCorre D, Bras J, Dufresne A (2011) Evidence of micro- and nanoscaled particles during starch nanocrystals preparation and their isolation. Biomacromolecules 12:3039–3046

Montalbo-Lomboy M, Khanal SK, Van Leeuwen JH, Raj Raman D, Grewell D (2011) Simultaneous saccharification and fermentation and economic evaluation of ultrasonic and jet cooking pretreatment of corn slurry. Biotechnol Prog 27:1561–1569

Mullick A, Neogi S (2018) Acoustic cavitation induced synthesis of zirconium impregnated activated carbon for effective fluoride scavenging from water by adsorption. Ultrason Sonochem 45:65–77

Murshed SS, Tan SH, Nguyen NT (2008) Temperature dependence of interfacial properties and viscosities of nanofluid for droplet-based microfluidics. J Phys D Appl Phy 41(8):1–16

Nara S, Komiya T (1983) Studies on the relationship between water saturated state and crystallinity by the diffraction method for moistened potatoes starch. Starch-Starke 35(12):407–410

Nitayavardhana S, Shrestha P, Rasmussen ML, Lamsal BP, Van Leeuwen JH, Khanal SK (2010) Ultrasound improved ethanol fermentation from cassava chips in cassava based ethanol plants. Bioresour Technol 101:2741–2747

O'Sullivan J, Murray B, Flynn C, Norton I (2016) Effect of ultrasound treatment on the structural, physical and emulsifying properties of animal and vegetable protein. Food Hydrocolloids 53:141–151

Ogunlaja S, Pal R, Sarikhani K (2017) Effects of starch nanoparticles on phase inversion of pickering emulsions. Can J Chem Eng 9999:1–9

Pei H, Zhang G, Ge J, Jin L, Ma C (2013) Potential of alkaline flooding to enhance heavy oil flooding recovery through water-in-oil emulsification. Fuel 104:284–293

Pei X, Zhai K, Liang X, Deng Y, Tan Y, Wang P, Xu K (2017) Interfacial activity of starch-based nanoparticles at the oil-water interface. Langmuir 33(15):3787–3793

Qin Y, Liu C, Jiang S, Xiong L, Sun Q (2016) Characterisation of starch nanoparticles prepared by nanoprecipitation: influence of amylose content and starch type. Ind Crops Prod 87:182–190

Saha R, Uppaluri RV, Tiwari P (2018) Silica nanoparticle assisted polymer flooding of heavy crude oil: emulsification, rheology and wettability alteration characteristics. Ind Eng Chem Res 57(18):6364-63-76

Shahrodin NS, Rahmat AR, Arsad A (2015) Synthesis and characterisation of cassava starch nanocrystals by hydrolysis method. Adv Mater Res 1113:446–452

Strand S, Hognesen E, Tor Austad (2006) Wettability alteration of carbonates-effects of potentially determining ions (Ca^{2+} and SO_4^{2-}) and temperature. Colloids Surf A Physicochem Eng Aspects 275:1–10

Suslick KS (2001) Sonoluminescence and sonochemistry. In: Meyers RA (ed) Encyclopedia of physical science and technology. Academic, San Diego

Velmurugan R, Muthukumar K (2012) Sono-assisted enzymatic saccharification of sugarcane bagasse for bioethanol production. Biochem Eng J 63:1–9

Wang B, Zhang Z, Chang K, Cui J, Rosenkranz A, Yu J, Lin C, Chen G, Zang K, Luo J, Jiang N, Guo D (2018) New deformation-induced nanostructure in silicon. Nano Lett 18(7):4611–4617

Ye F, Miao M, Lu K, Jiang B, Li X, Cui S (2017) Structure and physicochemical properties of modified starch-based nanoparticles from different maize properties. Food Hydrocolloids 67:37–44

Yekeen N, Padmanabhan E, Idris AK (2019) Synergistic effects of nanoparticles and surfactants on n-decane-water interfacial tension and bulk foam stability at high temperature. J Pet Sci Eng 179:814–830

Zargartalebi M, Kharrat R, Barati M (2015) enhancement of surfactant flooding performance by the use of silica nanoparticles. Fuel 143:21–27

Zetasizer Nano Series User Manual (2015) Malvern instruments: Vol. MAN0317, Iss. 2.2

Zhang Z, Huo F, Zhang X, Guo D (2012a) Fabrication and size prediction of crystalline nanoparticles of silicon induced by nanogrinding with ultrafine diamond grits. Scripta Mater 67:657–660

Zhang Z, Song Y, Huo F, Guo G (2012b) Nanoscale material removal mechanism of soft-brittle HgCdTe single crystals under nanogrinding by ultrafine diamond grits. Tribol Lett 46:95–100

Zhang Z, Song Y, Xu C, Guo D (2012c) A novel model for undeformed nanometer chips of soft-brittle HgCdTe films induced by ultrafine diamond grits. Scripta Mater 67(2):197–200

Zhang Z, Huo Y, Guo D (2013a) A model for nanogrinding based on direct evidence of ground chips of silicon wafers. Sci China Technol Sci 56(9):2099–2108

Zhang Z, Zhang X, Xu X, Guo D (2013b) Characterization of nanoscale chips and a novel model for face nanogrinding on soft-brittle HgCdTe films. Tribol Lett 49:203–215

Zhang Z, Wang B, Kang R, Zhang B, Guo D (2015a) Changes in surface layer of silicon wafers from diamond scratching. CIRP Ann Manuf Technol 64:349–352

Zhang Z, Guo D, Wang B, Kang R, Zhang B (2015b) A novel approach of high speed scratching on silicon wafers at nanoscale depths of cut. Sci Rep 5:16395

Zhang Z, Wang B, Zhou P, Guo D, Kang R, Zhang B (2016) A novel approach of chemical mechanical polishing using environment-friendly slurry for mercury cadmium telluride semiconductors. Sci Rep 6:22466

Zhang Z, Huang S, Chen L, Wang B, Wen B, Zhang B, Guo D (2017a) Ultrahigh hardness on a face-centered cubic metal. Appl Surf Sci 416:891–900

Zhang Z, Cui J, Wang B, Wang Z, Kang R, Guo D (2017b) A novel approach of mechanical chemical grinding. J Alloy Compd 726:514–524

Zhang Z, Shi Z, Du Y, Yu Z, Guo L, Guo D (2018) A novel approach of chemical mechanical polishing for a titanium alloy using an environment-friendly slurry. Appl Surf Sci 427:409–415

Zhang Z, Cui J, Zhang J, Liu D, Yu Z, Guo D (2019) Environment friendly chemical mechanical polishing of copper. Appl Surf Sci 467–468:5–11

مدينة الملك عبدالعزيز
KACST للعلوم والتقنية

Springer